








# Fusion of Optical and Radar Data by Aggregation into a Single Feature Space for LULC Classification

Veronica Herrera-Ruiz<sup>1</sup> , Jheison Perez-Guerra<sup>1</sup> ,  
Juan David Martínez-Vargas<sup>2</sup> , Juan Carlos Gonzalez-Velez<sup>1</sup> ,  
and Maria Constanza Torres-Madronero<sup>1</sup> 

<sup>1</sup> Department of Engineering, MIRP Research Group, Institución Universitaria ITM,  
Medellín, Colombia

veronicaherrera239462@correo.itm.edu.co

<sup>2</sup> Universidad EAFIT, Medellín, Colombia

**Abstract.** Land use and land cover classification (LULC) is a fundamental input for ecological and socioeconomic models worldwide, generating a large volume of data from space-based platforms, mainly optical technologies. However, these can be affected by atmospheric conditions. Colombia has a high percentage of cloud cover due to its geographical location, which makes it challenging to map LULC changes. Studies have emerged that evaluate the integration of optical and radar images with algorithms that allow for good results despite the information gaps that affect these processes. Therefore, this work compares three supervised machine learning approaches, Support Vector Machines, Random Forest, and XGBoost, to classify land use and land cover from multispectral and radar images, contemplating four scenarios for data fusion. Optical, optical + SAR, optical + SAR ascending, and optical + SAR descending. The result for the Random Forest model using optical + ascending SAR has the best accuracy (76.02%), followed by Random Forest with optical + descending SAR data (75.97%) and with little difference for Random Forest using optical data (75.83%). In future studies, it is of great interest to explore feature extraction on both data sets to improve LULC representation and classification.

**Keywords:** Land Use Land Cover · Classification · Machine Learning · Remote sensing · Multispectral images · Fusion data

## 1 Introduction

Natural resources in the world are excessively exploited by human beings to satisfy subsistence needs, such as food, health, economy, and leisure [1]. However, the great tendency of waste and over-exploitation of these resources produces severe consequences for the planet year after year. Some of the human activities that cause these effects are the expansion of the agricultural frontier, livestock,

infrastructure, and mining, in addition to other indirect causes associated with social, political, and economic changes [2]. Thus, the care and evolution of natural resources have awakened great interest in generating information and knowledge on land use, land cover, and its changes over time, representing a great need in the scientific community [3].

Large volumes of remote sensing data are produced annually from various systems, also associated with many Earth observation satellites used to monitor activities related to land use and land cover [4]. This increased availability of remotely sensed data has led to a rapid advance and interest in the fusion of optical and radar data. Whereas optical sensors are passive and receive the solar electromagnetic waves reflected from objects to obtain spatial and spectral information, while synthetic aperture radar (SAR) is active, and its images are not affected by weather conditions or sunlight levels [4, 5], which together allow obtaining the best of both and complement each other's deficiencies [6]. However, this data fusion has not yet received sufficient attention.

For LULC processing and classification, multiple algorithms have been studied; among these, machine learning (ML) techniques are one of the most relevant [7]. This technique seeks to extract knowledge from the data. Its main objective is to find models that can identify patterns to obtain more secure and reliable classifications [3]. In studies on supervised methods in classification applications, Support Vector Machines (SVM), Random Forest (RF), and Extreme Gradient Boosting (XGBoost) are reported as the most popular ones [8]. Since these generally provide better performance than other traditional classifiers [9]. Furthermore, it is valuable to highlight the potential of machine learning to deal with large historical and current data sets, which are indispensable in applying these algorithms for LULC analysis and classification [10].

Therefore, the purpose of this study is to identify the possibility of increasing the performance of the LULC classification through the fusion of optical and radar data in areas with a high percentage of clouds. It is hoped that this fusion will allow for mitigating the deficiency in data acquisition with optical sensors due to atmospheric conditions in Colombia, a country in which these studies are currently minimal. Initially, the use of 4 of the 5 classes specified in Level 1 of CORINE Land Cover (CLC) is proposed to allow a generic exploration of very common areas in the territory; some examples are artificialized territories (urban areas), agricultural territories (crops), forests and semi-natural areas (pastures), and water surfaces (watercourses).

## 2 Methods

This research used the main steps of the methodology shown in Fig. 1 to examine land cover classification and analysis from radar and optical data:

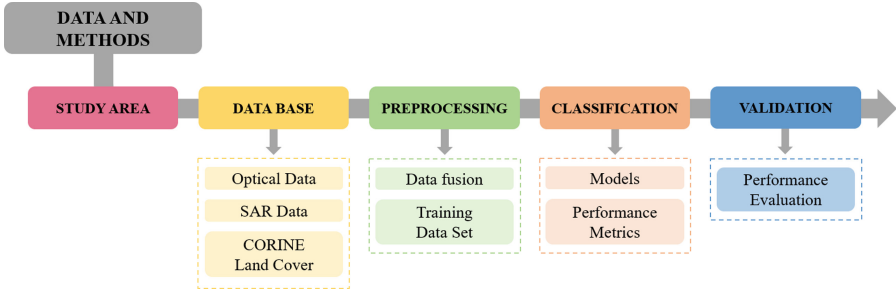


Fig. 1. Data and Methods. Source: Created by Authors.

## 2.1 Study Area

The study area chosen for this research is located in Antioquia, Colombia. It covers approximately 190,000 hectares of widely diversified territory and is better known as the Oriente Antioqueño sub-region, precisely between the municipalities of Guarne, Guatapé, La Ceja, and Cocorná.

## 2.2 Data Base

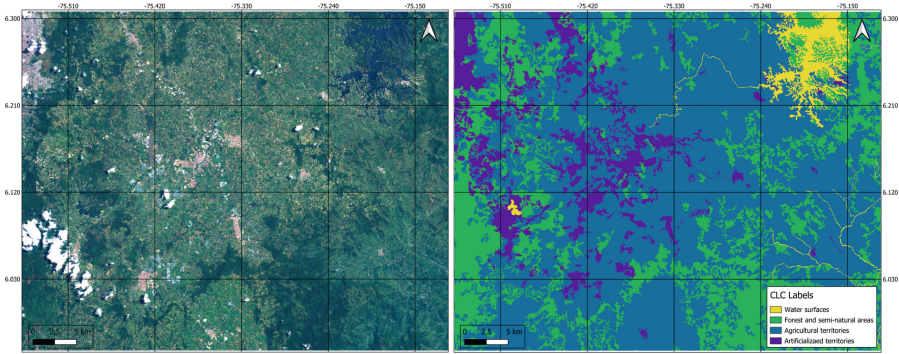
The database comprises optical images from the Sentinel 2 sensor and SAR images from the Sentinel 1 sensor, taken as of August 2019. For Sentinel 2 data, we used the bands with spatial resolution below 20 m and level 2 A (i.e., the orthorectified image with reflectance levels below the atmosphere). While for Sentinel 1, the data were taken from the Ground Range Detected (GRD) collection in vertical transmit and receive (VV) and vertical transmit and horizontal receive (VH) polarization, each in ascending and descending orbit. Resampling was performed for both datasets using the Google Earth Engine tool so that the Sentinel 2 bands were all taken to 20 m, as were the SAR data.

Table 1 details the satellite images and sensors used for the different tasks in this study.

Table 1. Optical and SAR data details

	Sensor	Number of bands	Date	Download Source
Optical	Sentinel 2	10	2019	Google Earth Engine
SAR	Sentinel 1	4	2019	Google Earth Engine

**CORINE Land Cover.** As reference data to validate the process, the CORINE Land Cover (CLC) methodology map currently led in Colombia by the Institute of Hydrology, Meteorology and Environmental Studies (IDEAM) is considered, which includes land cover classifications obtained from the visual interpretation of expert cartographers, detailed from level 1 to level 6. For this study, 4 of the 5 classes defined at level 1 (artificialized territories (ArT), agricultural territories (AgT), forests and semi-natural areas (FSA), wetlands and water surfaces (WS)) are taken, as shown in Fig. 2.



**Fig. 2.** Study Area & CLC Classes. Source: Created by Authors.

### 2.3 Preprocessing

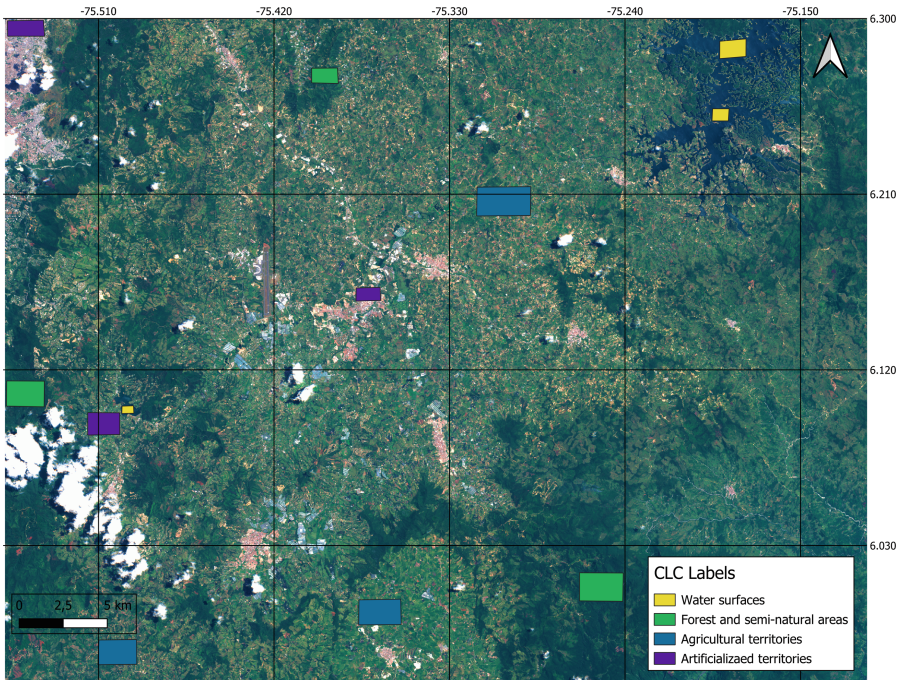
The data preparation generally included the construction of the data sets for each image, organizing the matrices of equal length and order according to the bands of each sensor; additionally, all the data were normalized using the Min-MaxScaler function and divided in a relation of 70% training and 30% test using the `train_test_split` function.

**Data Fusion.** The pixel values of each image were used for data fusion, considering four scenarios: Optical, Optical + SAR, Optical + ascending SAR, and Optical + descending SAR. The fusions' composition details can be seen in Table 2.

**Training Data Set.** The information for the training dataset is initially structured using the QGIS Geographic Information System software. Multiple slices of the image are extracted in specific areas so that each class of interest is properly identified, as can be seen in Fig. 3.

**Table 2.** Composite Images

Composite Images	Bands
Optical	B2, B3, B4, B5, B6, B7, B8, B8A, B11, and B12
SAR	VV ascending, VV descending, VH ascending, and VH descending
Optical + SAR	B2, B3, B4, B5, B6, B7, B8, B8A, B11, B12, VV ascending, VH ascending, VV descending, VH descending
Optical + SAR Ascending	B2, B3, B4, B5, B6, B7, B8, B8A, B11, B12, VV ascending, VH ascending
Optical + SAR Descending	B2, B3, B4, B5, B6, B7, B8, B8A, B11, B12, VV descending, and VH descending

**Fig. 3.** Training Data Sets. Source: Created by Authors.

## 2.4 Classification

**Models.** Three models with supervised machine learning approaches, all set in classification mode, were used for comparison. The first one is SVM which behaves as a tool that maximizes prediction accuracy by automatically avoiding overfitting the data. It seeks to find hyperplanes that determine the decision boundary to classify data points into different classes [11, 12]. In addition to supporting multiple continuous and categorical variables and linear and nonlinear samples. The training samples that constrain the margin or hyperplane are the

support vectors [7]. The second model is RF which consists of a collection of tree-structured classifiers with identically distributed independent random vectors, where, each tree casts a unitary vote for the most popular class of the input, allowing to obtain a more accurate and stable prediction [6,7]. Finally, XGBoost with a concurrent tree boosting approach provides more accurate large scale problem solving. [8] A classifier is constructed from gradient boosting that predicts a new classification membership after each iteration in an additive manner, making predictions from a weak tree that constantly improves the error of previous classifiers to create a robust classifier [13].

## 2.5 Validation

### Performance Evaluation

*Confusion Matrix (CM)*. A tool for visualizing the performance of an algorithm used in supervised learning, it contains information about the actual and predicted classifications performed by the classification system (See Fig. 4). The performance of these systems is usually evaluated using the matrix data itself [14].

Actual	True Positive	False Positive
	False Negative	True Negative
		Predicted

**Fig. 4.** Confusion matrix. Source: Created by Authors.

*Accuracy*. It is a metric widely used to evaluate classification models, where the probability that a sample is correctly classified is established: the sum of true positives plus true negatives divided by the total number of samples analyzed [6].

$$Accuracy = \frac{TruePositive + TrueNegative}{AllSamples} \quad (1)$$

## 3 Result and Discussion

The results obtained for the database are shown in the Table 3 with the number of records for each class according to the training and validation test respectively. The number of records is equal for each of the 4 data sets.

The classification of optical images, SAR, and the fusion of both was performed using Random Forest, Support Vector Machine, and XGBoost algorithms. The parameters established for the models were the following: SVM

with Kernel Radial Basis Function ('rbf'), RF with a maximum depth of the tree at 2 and Random State at 0, and XGBoost was set for multiple classes using the softmax objective and Random State at 42.

The best accuracies obtained were using the Random Forest model, specifically with optical data + ascending SAR (76.02%), followed by optical data + descending SAR (75.97%), and with little difference continued with optical data (75.83%). Table 4 shows the comparison of accuracies according to the data set and each model. Overall over the data sets, the classification using optical imaging + SAR was surprisingly the least accurate, very close to the optical imaging set; however, when considering the difference in data by orbit, the accuracy using optical imaging + ascending SAR increased.

**Table 3.** Database Size

Class	Train	Test
ArT	12819	460853
AgT	28961	2960360
FSA	20826	1240530
WS	5991	149005
<b>Total</b>	<b>68597</b>	<b>4810748</b>

**Table 4.** Comparison of Model Accuracy

Data	Model	Accuracy
Optical	RF	75,83%
Optical	XGB	68,91%
Optical	SVM	75,27%
Optical + SAR	RF	75,59%
Optical + SAR	XGB	69,80%
Optical + SAR	SVM	75,19%
<b>Optical + SAR Ascending</b>	<b>RF</b>	<b>76,02%</b>
Optical + SAR Ascending	XGB	69,19%
Optical + SAR Ascending	SVM	75,17%
<b>Optical + SAR Descending</b>	<b>RF</b>	<b>75,97%</b>
Optical + SAR Descending	XGB	69,47%
Optical + SAR Descending	SVM	75,25%

Figure 5 shows the classification maps obtained using the RF model with the Optical, SAR Ascending, and Descending images, respectively, to allow visual

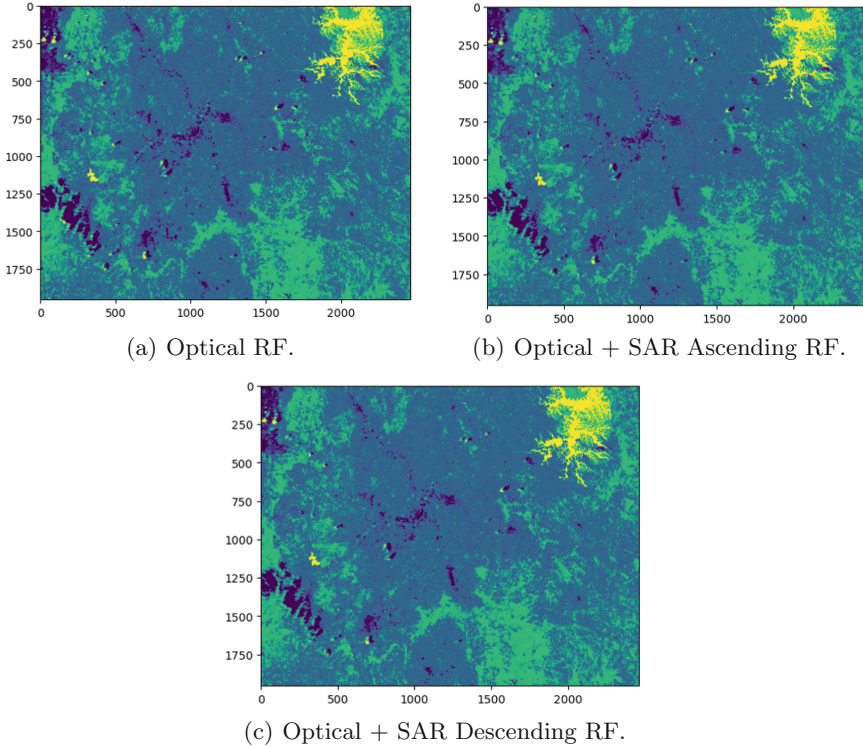


**Fig. 5.** Images of predictions. Source: Created by Authors.

comparison of the effectiveness of the different dataset approaches that obtained the best accuracy.

With the optical data, it can be identified that the presence of clouds does indeed affect the predictions, and these are classified on the map as artificialized territories; however, the shadows produced by these are also classified, but in this case, as primarily water surfaces. Meanwhile, with the fusion of optical and SAR data, a visually improved land cover map was obtained since the pixels erroneously classified by the phenomenon of cloudiness was reduced.

Figure 6 presents the confusion matrices for the three best results obtained with RF mentioned above. The number of correct classifications is shown in the diagonals in dark green shades. For example, 2537175 optical pixels were correctly classified as AgT, while for the merged data, it increases to around 40000 samples, respectively. It is also identified that this class is the most preponderant in all the classifications obtained, possibly because of the specific properties that differentiate it from the others. In turn, the second best-predicted class is WS, where the class has about 75,4% equivalent to 112395 correctly sorted samples, specifically in optical data.



**Table 5.** Label abbreviation

ArT	Artificialized territories
AgT	Agricultural territories
FSA	Forests and semi-natural areas
WS	Water surfaces

True Class	ArT	131852 (28,6%)	307885	17702	3414
	AgT	123377	2537175 (85,7%)	293551	6257
	FSA	40014	330412	862738 (69,5%)	7366
	WS	2749	20623	13238	112395 (75,4%)
	Predicted Class	ArT	AgT	FSA	WS

(a) CM optical data.

True Class	ArT	115913 (25,1%)	324915	17034	2991
	AgT	90914	2580315 (87,1%)	284529	4602
	FSA	33932	355112	845415 (68%)	6071
	WS	1738	24365	11032	111870 (75%)
	Predicted Class	ArT	AgT	FSA	WS

(b) CM optical + SAR Ascending data.

True Class	ArT	115912 (25,1%)	324732	17222	2987
	AgT	90914	2578954 (87,1%)	285829	4663
	FSA	33932	352631	847883 (68,3%)	6084
	WS	1738	23098	12318	111851 (75%)
	Predicted Class	ArT	AgT	FSA	WS

(c) CM optical + SAR Descending data.

**Fig. 6.** Confusion matrix of predictions. Source: Created by Authors.

## 4 Conclusion

This research fused optical and SAR imagery for LULC classification using machine learning algorithms and evaluates the accuracy of maps obtained with optical imagery, SAR, and the combination of both.

The accuracy of the map obtained using optical and SAR imagery was superior to that obtained with optical imagery alone, demonstrating that better land cover classification can be obtained by providing details from both systems that allow them to complement each other. However, there is still an increase in the error of the classifications due to the presence of clouds in the optical data, for which it is

necessary to advance in the investigation of techniques to reduce the interference of these clouds in the information provided by the data characteristics.

Finally, this research presents baseline results that can be used to give continuity to the analysis of multisensory data fusion techniques and optimization of supervised models for LULC classification (Table 5).

## References

1. Salas, J.A.O., Portilla, T.D.C.L.: Uso e importancia de los recursos naturales y su incidencia en el desarrollo turístico. Caso Cantón Chilla, El Oro, Ecuador Use and importance of the natural resources and their impact on tourism development. Case of Chilla Canton, El Oro, Ecuador. *Revista Interamericana de Ambiente y Turismo* **14**, 65–79 (2018)
2. Constanza, M., Armenteras, D.: Uso del suelo y estructura de la vegetación en paisajes fragmentados en la amazonia, Colombia. *Colombia Forestal* **21**(2), 205–223 (2018)
3. Mancera Florez, J.: Evaluación de imágenes de radar Sentinel- 1A e imágenes multiespectrales Sentinel-2A en la clasificación de cobertura del suelo en diferentes niveles de detalle. Ph.D. dissertation (2019)
4. Chen, Y., Bruzzone, L.: Self-supervised SAR-optical data fusion and land-cover mapping using sentinel-1/-2 images, no. Mcl, pp. 1–10 (2021). <http://arxiv.org/abs/2103.05543>
5. Yuan, Y., et al.: Multi-resolution collaborative fusion of SAR, multispectral and hyperspectral images for coastal wetlands mapping. *Remote Sens.* **14**(14), 1–27 (2022)
6. Nhemaphuki, D., Thapa Chetri, K., Shrestha, S.: Fusion of radar and optical data for land cover classification using machine learning approach. *J. Geoinform.* **20**(1), 39–45 (2020)
7. Talukdar, S., et al.: Land-use land-cover classification by machine learning classifiers for satellite observations-a review. *Remote Sens.* **12**(7) (2020)
8. Shakya, A., Biswas, M., Pal, M.: Fusion and classification of SAR and optical data using multi-image color components with differential gradients. *Remote Sens.* **15**(1) (2023)
9. Lapini, A., Pettinato, S., Santi, E., Paloscia, S., Fontanelli, G., Garzelli, A.: Comparison of machine learning methods applied to SAR images for forest classification in mediterranean areas. *Remote Sens.* **12**(3) (2020)
10. Basheer, S., et al.: Comparison of land use land cover classifiers using different satellite imagery and machine learning techniques. *Remote Sens.* **14**(19), 1–18 (2022)
11. Ouma, Y., et al.: Comparison of machine learning classifiers for multitemporal and multisensor mapping of urban LULC features. *Int. Arch. Photogrammetry Remote Sens. Spatial Inf. Sci. - ISPRS Arch.* **43**(B3–2022), 681–689 (2022)
12. Thyagarajan, K.K., Vignesh, T.: Soft computing techniques for land use and land cover monitoring with multispectral remote sensing images: a review. *Arch. Comput. Methods Eng.* **26**(2), 275–301 (2019)
13. Georganos, S., Grippa, T., Vanhuysse, S., Lennert, M., Shimoni, M., Wolff, E.: Very high resolution object-based land use-land cover urban classification using extreme gradient boosting. *IEEE Geosci. Remote Sens. Lett.* **15**(4), 607–611 (2018)
14. Shultz, T.R., Fahlman, S.E.: *Encyclopedia of Machine Learning and Data Mining* (2017)